PCP-dependent transcellular regulation of actomyosin oscillation facilitates convergent extension of vertebrate tissue

Asako Shindo[a,c,*,1], **Yasuhiro Inoue**[1,b], **Makoto Kinoshita**[a], and **John B. Wallingford**[c]

[a]Division of Biological Sciences, Department of Molecular Biology, Graduate School of Science, Nagoya University, Nagoya, 464-8602, Japan.

[b]Institute for Frontier Life and Medical Sciences, Kyoto University, Kyoto, 606-8507, Japan

[c]Department of Molecular Biosciences, University of Texas at Austin, 78712, USA.

Abstract

Oscillatory flows of actomyosin play a key role in the migration of single cells in culture and in collective cell movements in *Drosophila* embryos. In vertebrate embryos undergoing convergent extension (CE), the Planar Cell Polarity (PCP) pathway drives the elongation of the body axis and shapes the central nervous system, and mutations of the PCP genes predispose humans to various malformations including neural tube defects. However, the spatiotemporal patterns of oscillatory actomyosin contractions during vertebrate CE and how they are controlled by the PCP signaling remain unknown. Here, we address these outstanding issues using a combination of *in vivo* imaging and mathematical modeling. We find that effective execution of CE requires alternative oscillations of cortical actomyosin across cell membranes of neighboring cells within an optimal frequency range. Intriguingly, temporal and spatial clustering of the core PCP protein Prickle 2 (Pk2) is correlated to submembranous accumulations of F-actin, and depletion of Pk2 perturbs the oscillation of actomyosin contractions. These findings shed light on the significance of temporal regulation of actomyosin contraction by the PCP pathway during CE, in addition to its well-studied spatial aspects.

Keywords

Actomyosin oscillation; Convergent extension; Planar cell polarity; Cell intercalation; Prickle 2

*Corresponding author and Lead Contact: Nagoya University, Chikusa-ku Furo-cho, Nagoya, Aichi, Japan 464-8602, +81-52-789-2508; shindo.asako@f.mbox.nagoya-u.ac.jp.
[1]Equal contribution

1. Introduction

Convergent extension (CE) is a ubiquitous process of collective cell movement that elongates the body axis in animals (Tada and Heisenberg, 2012). During convergent extension, cells rearrange by intercalating specifically in the mediolateral axis, thereby elongating the tissue in the perpendicular, anteroposterior axis (Walck-Shannon and Hardin, 2014). Two sub-cellular mechanisms have been shown to contribute to mediolateral cell intercalation (Shindo, 2017): First, mediolaterally-oriented protrusions act in a manner analogous to the leading edge of a migrating cell, driving cell intercalation via cell crawling (Shih and Keller, 1992). Second, pulsed actomyosin contractions actively shrink mediolaterally-oriented junctions (so called v-junctions, Figure S1A), thereby driving intercalation (Bertet et al., 2004, Blankenship et al., 2006, Rauzi et al., 2008). Recent work suggests that these two mechanisms act in concert in both vertebrates and *Drosophila* (Williams et al., 2014, Sun et al., 2017, Huebner and Wallingford, 2018).

Actomyosin contraction is the key driver of animal cell movement (Gardel et al., 2010), so understanding how the actomyosin machinery is organized during CE is an important challenge. In the context of CE, this issue is currently best understood for junction shrinking in the epithelial cells of the *Drosophila* germband, a key model system for studies of cell intercalation (Bertet et al., 2004, Blankenship et al., 2006). In that case, two populations of actin have been shown to act in concert: Oscillation of a pool of "medial" actin drives pulsed constriction events at the junction, and oscillations of a second pool of "junctional" actin stabilizes the newly-shortened junction (Fernandez-Gonzalez and Zallen, 2011, Rauzi et al., 2010, Sawyer et al., 2011).

Cell intercalation has also been extensively studied in the mesenchymal cells of the *Xenopus* gastrula mesoderm (Figure S1B)(Keller et al., 2000), though how actomyosin dynamics relate to cell intercalation in these cells is far less clear. As in the *Drosophila* germband, two actin populations have been described in the *Xenopus* mesoderm during CE. First, there is a "node-and-cable" system of actin filaments that resides superficially (i.e. 1–2 μm deep; Figure S2A, A') and displays oscillations that are implicated in cell intercalation by cell crawling (Kim and Davidson, 2011, Pfister et al., 2016, Skoglund et al., 2008). In addition, we have described a pulsatile actin population associated with junction shrinkage deeper within the tissue (4–6 μm; Figure S2B, B')(Shindo and Wallingford, 2014). Here, we will refer to these as the "superficial" and "deep" actin populations, respectively. The relationship between these two actomyosin populations remains unclear.

Understanding actomyosin dynamics during CE in a vertebrate is crucial, because Planar Cell Polarity (PCP) signaling is an essential regulator of cell intercalation specifically in vertebrates (Butler and Wallingford, 2017) and not in *Drosophila* (Zallen and Wieschaus, 2004). Moreover, CE is essential for normal neural tube closure in vertebrates and PCP genes are key genetic risk factors for human neural tube closure defects (Wallingford et al., 2013). PCP proteins control myosin phosphorylation and disruption of PCP signaling severely disrupts myosin-mediated junction shrinking in diverse tissues, including the *Xenopus* mesoderm (Butler and Wallingford, 2017). However, despite the wide-spread implication of actomyosin oscillation and flow in morphogenesis of invertebrates (He et al.,

2010, Fernandez-Gonzalez and Zallen, 2011, Martin et al., 2009, Rauzi et al., 2010, Sawyer et al., 2011) and in migration of single vertebrate cells in culture (Huang et al., 2013, Maiuri et al., 2015), we understand little about the spatial and temporal dynamics of actomyosin and how these are influenced by PCP proteins during vertebrate collective cell movement.

In this study, we performed high-resolution, three-dimensional time-lapse imaging of actin and myosin dynamics during CE in the dorsal gastrula mesoderm of *Xenopus*. We adopted a mathematical modeling approach to ask how the observed patterns of actomyosin behavior may impact cell intercalation during CE. Together with the previous findings in *Drosophila*, our findings *in silico* and in *Xenopus* gastrulae *in vivo* argue that oscillatory actomyosin contraction is a general principle of cell intercalation via junction shrinking that is conserved across cell types and animals. We also show that in addition to its known role in controlling the planar orientation of actomyosin contraction, PCP signaling is required to tune the frequency of those oscillatory contractions. These results shed light on the molecular mechanisms of CE and of congenital diseases related to defective PCP signaling.

2. Results

2.1. Synchronized oscillation links intracellular actomyosin populations during convergent extension of the *Xenopus* mesoderm.

We first asked if the dynamics of the superficial "node-and-cable" system of actin filaments and the deep pulsatile actin population associated with junction shrinkage in a vertebrate CE *in vivo* using the dorsal mesoderm of *Xenopus laevis* (Figure S1C, D). Using 3D time-lapse imaging to simultaneously monitor the superficial and deep actin pools, we found that the two oscillate synchronously within individual cells during junction shrinking (Figure 1A, Movie S1). To quantify this oscillatory behavior, we identified actin flows as the peaks of normalized fluorescent intensity over time (Figure S3), and this analysis revealed that actin pulses initiated in the deep population at shrinking cell-cell junctions and then flowed to the superficial actin pool (Figure 1B). Cross-correlation of the data confirmed the synchrony of deep and superficial actin pulses, with the peak of superficial actin intensity following the peak of deep actin by ~20 seconds on average (Figure 1C, max of cross-correlation coefficient: 0.404 ± 0.154 (mean $\pm$ sd)).

We previously reported that the myosin regulatory light chain 9 (Myl9) oscillates with the deep junctional pool of F-actin at the shrinking-junctions during CE (Shindo and Wallingford, 2014). When co-expressed with LifeAct-RFP, a F-actin marker, and membrane (Mem) -BFP, we found that Myl9-GFP also oscillated with F-actin in the superficial population (Figure S4A, Movie S2). Cross-correlation analysis between the intensity of Myl9-GFP and LifeAct-RFP indicated a synchronized oscillation of Myl9 and F-actin in these two populations (Figure S4A', max of cross-correlation coefficient: 0.728766 ± 0.051 (mean $\pm$ sd)). These results suggest that oscillatory actomyosin contractions are synchronized within individual cells during CE.

2.2. Anteroposterior neighbor cells display asynchronous intercellular actomyosin oscillations during convergent extension.

Our data suggest that deep and superficial actomyosin flows are synchronized *within* individual cells during convergent extension, so we next asked how the flows are coordinated *between* neighboring cells. Because of the known relationship of anteroposterior neighbor cells in junction shrinking (Shindo and Wallingford, 2014), we used a two-color imaging approach to unambiguously assess actomyosin dynamics at the cell-cell junction between anteroposteriorly neighboring cells (Figure. S1D, S1D'). Time-lapse imaging demonstrated that actin and Myl9 flows in anteroposterior neighbors displayed asynchronous oscillations (Figure 1D, 1D', S4B). These oscillations appeared anti-correlated in time-lapse movies (Figure 1D) and kymographs (Figure S5). However, their timing was highly variable, precluding determination of cross-correlation on average (Figure S4B'). Nonetheless, quantification of the relative timing of pulses (Figure S6) revealed a dominant one-to-one ratio of oscillations between neighboring cells (Figure 1E), suggesting a predominantly alternating relationship between neighboring cells. Thus, oscillations are synchronous between the deep and superficial actomyosin populations *within* each cell, but oscillations *between* cells are asynchronous.

2.3. Mathematical modeling suggests that asynchronous contractile oscillations with an optimal frequency increase the efficiency of convergent extension.

Understanding the significance of actomyosin dynamics in embryos is challenging because collective cell movements emerge *in vivo* from the coordination of actomyosin contractile systems both within cells and between cells as we observed (Guillot and Lencuit, 2013, Heisenberg and Bellaiche, 2013, Mao and Baum, 2015). In regard to this issue, mathematical modeling provides a powerful tool for understanding such complexities (Alt et al., 2017, Yu and Fernandez-Gonzalez, 2017, Inoue et al., 2016, Szabó et al., 2016). Thus, we adopted mathematical modeling as an amenable way to test for potential benefits of the spatiotemporal patterns of actomyosin oscillation for CE.

We modified the 2D vertex model, in which cell-cell junctions are modeled as two vertices and one edge shared by neighboring cells. We considered two factors, orientation and oscillation, for the line tension in the model (See method). The orientation factor limited contraction to edges aligned along the x-axis, representing the mediolateral contraction of cell-cell junctions (Figure 2A, A'). The oscillatory factor allowed us to manipulate the pattern of oscillations across multiple cells. By utilizing our modified 2D vertex model, we modeled junction shrinking with tension exerted along edges, thereby reducing the distance between vertices (Farhadifar et al., 2007, Staple et al., 2010). We then quantified the efficiency of CE by counting the number of new edges emerging after complete shrinking of a v-junction, which represents cellular intercalation (Figure 2B).

We first tested the significance of oscillating contractions by simulating continuous contraction of v-junctions (Figures 2C, S7A), and strikingly, cells completely failed to intercalate (Figures 2C, 2G (blue), and S7A, Movie S3). By contrast, adding a synchronous oscillation of contractions (i.e. all cells oscillate in phase, Figure S7B) resulted in substantial cell intercalation (Figures 2D, 2G (black); Movie S3). We noted that even with synchronous

oscillations, the rate of cell intercalation eventually stalled, reaching a stable plateau beyond which no additional intercalation occurred (Figure 2D, 2G-black).

We therefore explored the role of contraction timing by comparing the effect of synchronous oscillations to that of alternating oscillations (Figure S7B, C). We found that alternating oscillations between neighboring cells along the y-axis (anteroposterior axis) resulted in significantly more cell intercalation than did synchronous contractions (Figures 2E, 2G-green, S7C, S7C', Movie S3). To probe the significance of this finding, we explored the interplay of oscillation timing and contraction strength. Interestingly, increasing the force of each contraction improved intercalation even in the absence of oscillations (Figure 2F, Movie S3), but importantly, it did not overcome the eventual plateau beyond which no more intercalation occurred (Figure 2G-orange). Without oscillations, the number of cell intercalations could not overcome this plateau even if we increase the force for edge contraction (data not shown). Thus, our model suggests that alternating contraction between neighboring cells that share a shrinking junction requires less tension, which allows cells to consume lower energy to generate contractile forces for CE.

Finally, our model provided us with the means to test the significance of contraction frequency in CE. We found that when alternating contraction oscillation was very rapid, intercalation either slowed or plateaued (Figure 2H, red and pink). Decreasing contraction frequency improved intercalation (Fig 2H, green), however only up to point; at very slow contractions frequencies, the progress of intercalation became irregular, showing a double plateau (Figure 2H, purple). Taken together, these simulations suggest that asynchronous and alternating oscillation, as well as tight control of contraction frequency, is important for CE by junction shrinking.

2.4. Prickle displays both spatial and temporal patterns of localization to cell-cell junctions during CE.

Both imaging and modeling data suggest that convergent extension requires the careful calibration of several parameters, including the frequency of contractile flows and their asynchronous coordination between neighboring cells. To explore the molecular control of these oscillations, we turned our attention to the PCP signaling network, which has been implicated in control of both deep and superficial actomyosin dynamics in the dorsal mesoderm (Kim and Davidson, 2011) (Shindo and Wallingford, 2014). In addition, we recently showed that the core PCP protein Pk2 controls CE in neural epithelial cells, where it displays a tight temporal and spatial correlation with actomyosin at shrinking junctions (Butler and Wallingford, 2018). We therefore used mosaic expression to generate labeled cells that were directly apposed to unlabeled cells in the dorsal mesoderm (Figure 3A). We then quantified the normalized fluorescence intensity at both anterior and posterior cell faces (Figure 3B, red, black). This analysis revealed that Pk2-GFP localized predominantly to the anterior face of cells engaged in CE (Figures 3C–3E, Movie S4). While this spatial localization of Pk2 is consistent with data in other cell types and organisms (Ciruna et al., 2006, Jiang et al., 2005, Ossipova et al., 2015, Yin et al., 2008), our dynamic imaging allowed us to detect additional *temporal* patterns.

For example, we found that junctional Pk2-GFP intensity was elevated specifically at shrinking junctions (Figures 3D–3E). Indeed, the increased junctional Pk2 intensity was significantly correlated with decreasing junction length (Figure 3F). Moreover, Pk2 intensity was also correlated with the angle Φ (Figure 3B, 3G), a cell-shape parameter that scales with the tension exerted on shrinking junctions during intercalation (Rauzi et al., 2008, Shindo and Wallingford, 2014). Further examination of Pk2 dynamics revealed a pulsatile pattern of junctional enrichment (Figure 3H), and we detected a significant cross-correlation between Pk2 intensity and actin intensity (Figure 3I, max of cross-correlation coefficient: 0.7155 ± 0.021 (mean ± sd)). Thus, Pk2 displays both spatial and temporal patterns of localization closely relating to junction shrinking during CE. These results are significant for providing the first time-resolved information about PCP protein localization during CE in the *Xenopus* mesoderm.

2.5. Prickle2 controls the frequency of actomyosin oscillations.

Finally, the coordinated pulsing of actomyosin and Pk2 is consistent with recent reports indicating a reciprocal relationship in which actomyosin controls PCP protein localization and PCP proteins in turn control myosin activity (Newman-Smith et al., 2015, Ossipova et al., 2015). Because we found that pulses of Pk2 were synchronized with those of F-actin, we tested the effect of Pk2 loss of function on the several parameters of actomyosin oscillation defined above (i.e. Figures 1 and 2). We knocked down Pk2 using an antisense morpholino-oligonucleotide that has been validated in both convergent extension and polarization of multiciliated cells (Butler and Wallingford, 2018, Butler and Wallingford, 2015). Pk2 knockdown disrupted both the elongation (Figures 4A, B, C) and the planar orientation (Figures 4A, B, D) of cells in the dorsal mesoderm, consistent with disruption of other core PCP proteins in dorsal gastrula mesoderm (Jessen et al., 2002, Wallingford et al., 2000). Interestingly, the effect on actomyosin was strikingly specific, as Pk2 knockdown did not eliminate oscillations (Figures 4E–4H), did not alter the tight relationship between actin and myosin (Figures 4I, 4I'), and did not disrupt the asynchronous nature of oscillations between neighboring cells (Figures 4J, S6, Movie S5). Instead, Pk2 knockdown affected the frequency of actomyosin contractions, with knockdown cells displaying an inter-peak time roughly half that of controls (Figures 4F, 4H, and 4K). Thus, our data suggest that Pk2 is required to tune the frequency of actomyosin oscillations, a parameter that our modeling suggests is essential for normal cell intercalation.

3. Discussion

In this study, we link the two populations of oscillating actomyosin in a cell, previously considered to be two distinct mechanisms for vertebrate CE (Kim and Davidson, 2011, Shindo and Wallingford, 2014). The live imaging reveals the asynchronous oscillations between neighboring cells during the cell junction shrinking, that is identified as a beneficial mode for CE in the simulations. Our simulation shows the frequency of the oscillation is also critical for CE. Finally, we identify the role of the PCP protein in controlling the frequency of actomyosin oscillation.

Oscillatory actomyosin contraction is a key feature of cell movement both in individual cells and in cell collectives, and such oscillations have been extensively defined during CE of the *Drosophila* germ band. However, CE is a ubiquitous morphogenetic process in animals, and we know little of such oscillatory contractions in other settings. The tightly cross-correlated flows between deep and superficial actin populations in the *Xenopus* dorsal mesoderm we observed within single cells are reminiscent of the flows between "medial" and "junctional" actin pools described in *Drosophila* (Rauzi et al., 2010, Sawyer et al., 2011). The asynchronous and alternate oscillations observed here between neighboring cells in *Xenopus* mesoderm are likewise reminiscent of similar patterns observed in *Drosophila* (Fernandez-Gonzalez and Zallen, 2011). Such similarities are highly significant because intercalations studied in *Drosophila* occur in tightly adherent epithelial cells with a well-defined apicobasal polarity, while the mesenchymal cells observed here in *Xenopus* are more loosely adherent and lack obvious apical-basal polarity. Moreover, CE in the *Xenopus* mesoderm is entirely dependent upon intact PCP signaling (Butler and Wallingford, 2017), but the analogous process in *Drosophila* is independent of this signaling system (Zallen and Wieschaus, 2004). Given these dramatic differences, the results of our imaging *in vivo* (Figure 1) and modeling *in silico* (Figure 2) strongly argue that asynchronous oscillatory contraction is a general principle of cell intercalation via junction shrinking that is conserved across cell types and animals.

Our data also provide important new insights into the function of PCP signaling in vertebrate CE, which is an important issue given the implication of PCP genes in human neural tube defects (Wallingford et al., 2013). The localization and dynamics of the Pk2 are consistent with our recent observations in neural epithelial cells (Butler and Wallingford, 2018), suggesting a common spatial and temporal pattern of Pk2 localization dynamics that spans cell fates (ectoderm vs. mesoderm) and tissue types (epithelial and mesenchymal). These results are also consistent with findings that anteroposterior patterning is central to the organization of CE in both *Drosophila* and *Xenopus* (Paré et al., 2014, Ninomiya et al., 2004, Zallen and Wieschaus, 2004). Regarding the positive feedback between the PCP protein and actomyosin contractility to localize them at the cell-cell junctions in neural epithelium (Ossipova et al., 2015, Newman-Smith et al., 2015), our data support the finding that their functions are tightly linked for shrinking cell-cell junction.

Previous work has implicated PCP signaling in control of both the deep and the superficial actin populations in the *Xenopus* dorsal mesoderm (Kim and Davidson, 2011, Shindo and Wallingford, 2014), so our finding that actomyosin flow links these two populations is informative. In fact, disruption of the core PCP protein Dvl reduces the frequency of superficial actin contractions in these cells (Kim and Davidson, 2011), suggesting that our finding of the opposite effect following Pk2 loss of function (Figure 4) is consistent with the antagonistic relationship between these two proteins in *Drosophila* (Jenny et al., 2005, Tree et al., 2002). Perhaps most significantly, we show here that Pk2 displays an oscillatory pattern of junctional enrichment that correlated with that of actomyosin in mesenchymal cells of the dorsal mesoderm (Figure 3). It is notable that regulatory molecules of actin are reported as the interactome of Pk2 (Paemka et al., 2015). Although the molecular sets functioning with Pk2 to regulate oscillation frequency remain to be identified, these data

suggest that the *temporal* patterns of PCP protein enrichment at cell-cell junction are at least as important as spatial patterns (i.e. planar asymmetry).

The mechanisms generating the alternating oscillations remain unknown. It is possible that the local interaction between the cells at the mediolaterally aligned cell junctions are involved, as a recent study combining imaging during *Drosophila* gastrulation and *in silico* approaches suggests that "asymmetric stiffness" of the two cell membrane at cell-cell junctions can attract or deplete motor proteins (Chanet et al., 2017). Adjacent contracted- and relaxed-cell membranes along the anteroposterior axis may be a basis for generating the alternating oscillations. It is also possible that the asynchronous contraction along mediolateral axis is necessary. Our model is designed to have the phase shift along both anteroposterior and mediolateral axes, raising the possibility that different timing of contractions along the mediolateral axis may also be important. This means that the alternating oscillation generates relaxed neighboring cells that can be pulled with smaller forces by the contracting cell-cell junction. The relationship between phase shift of anteroposterior and mediolateral axes will be an interesting property to investigate in the future for understanding the relationships between actomyosin oscillations and CE.

4. Materials and methods

4.1. Preparation of Xenopus embryos

Ovulation of adult *Xenopus laevis* females was induced by an injection of human chorionic gonadotropin. After incubating at 16 °C overnight, eggs were squeezed from the females, fertilized *in vitro* and dejellied in 3% cysteine (pH 7.8–8.0) at the two-cell stage. Fertilized embryos were washed and subsequently reared in 1/3 x Marc's Modified Ringer's (MMR) solution. To prepare the embryos for mRNA microinjections, the embryos were placed in 1/3 x MMR solution with 3% ficoll.

4.2. Plasmids and morpholino anti-sense oligonucleotides (MO)

GFP-Pk2 plasmids were constructed and designed as described previously in (Butler and Wallingford, 2015), and the Myl9-GFP plasmid in (Shindo and Wallingford, 2014). The Pk2 MO (GAACCCAAACAAACACTTACCTGTT) used disrupts splicing of the Pk2 gene (Butler and Wallingford, 2015) and severely disrupts CE of Keller explants and neural tube closure in intact *Xenopus* embryos; both phenotypes are rescued by co-expression of the wild-type Pk2 gene (Butler and Wallingford, 2018). Furthermore, these phenotypes are recapitulated by expression of a Pk2 dominant-negative (Butler and Wallingford, 2018) and are consistent with CE defects in a genetic mutant in the single *prickle* homolog in Ciona (Jiang et al., 2005).

4.3. Morpholino and mRNA microinjections

Capped mRNAs for fluorescent markers (GFP-Pk2, LifeAct-GFP, LifeAct-RFP, Myl9-GFP membrane-RFP, membrane-BFP) were synthesized using a mMessage mMachine kit (Thermo Fisher Scientific, Ambion). Morpholino (MO) or mRNA was injected into the two dorsal blastomeres targeting the dorsal marginal zone (DMZ). Pk2-MO was injected at 30 ng

per blastomere. The amounts of injected mRNAs per blastomere were as follows: GFP-Pk2 [90 pg], LifeAct-GFP/RFP [60 pg], Membrane-RFP/BFP [60 pg], Myl9-GFP [20 pg].

4.4. Live imaging of Keller explants

After mRNA injection, DMZ tissues were dissected out at stage 10.5 with forceps, hair loop, and hair knives (Figure S1C). The explants were mounted onto a fibronectin (Sigma, F1141) – coated glass bottom dish in DFA (Danilchik's for Amy) medium, and cultured at 13 °C for overnight. The explant imaging with a confocal microscope (CV1000, Yokogawa Electric Corporation) was started when the sibling embryos reached at stage 14–15. The time-lapse movie was taken every 10 sec for recording actomyosin pulsing.

4.5. Computational Simulation

We employ a 2D vertex model (Nagai T. and Honda 2001) to simulate the dynamics of multiple cells with cell rearrangement during convergent extension. In the model, cell shapes and their packing geometry are represented by a network of polygons consisting of vertices and edges. Cell rearrangement is expressed by implementing a local network topology change known as the T1 transition rule. The cell shape change is expressed by movements of vertices. The equation of motion of the i-th vertex at time t is

$$\eta \frac{d\mathbf{r}_i}{dt} = -\nabla_i U \quad (1)$$

where η is a frictional coefficient, and $\mathbf{r}_i$ is the position vector of the i-th vertex. The mechanical properties of the cells are expressed by an energy function U as follows.

$$U = \sum_\alpha \frac{K_\alpha}{2}\left(A_\alpha - A_\alpha^{(0)}\right)^2 + \sum_{(i,j)} \Lambda_{ij} l_{ij} + \sum_\alpha \frac{\Gamma_\alpha}{2} L_\alpha^2 \quad (2)$$

Here, the α-th cell's area A_α, perimeter L_α, and junctional length l_{ij} between the i-th and j-th vertices are represented as variables. The constants K_α and Γ_α are the area elasticity and peripheral contractility, respectively. The energy function U in Eq. (2) is basically the same as suggested in (Farhadifar et al., 2007) (Staple et al., 2010), while we redefine the line tension Λ_{ij} as a function of time and position of vertices to take into account a preferential direction of the oscillatory constriction at each individual cell described below.

The line tension Λ_{ij} on the junction line between i- and j-th vertices is decomposed to two contributions: orientation and oscillatory factors.

The orientation factor, p_{ij}, is introduced to express the mediolateral-oriented constriction.

$$p_{ij} = \left(\frac{\mathbf{e}_x \cdot \mathbf{l}_{ij}}{l_{ij}} \right)^2 \quad (3)$$

Here, $\mathbf{e}_x$ is the unit vector in the direction of the x-axis which is defined by the mediolateral axis (x axis in Figure 2A). The junctional line vector, $\mathbf{l}_{ij}$, is defined by the relative position vector from i-th to j-th vertices.

The oscillatory factor, $\Phi_a(t)$ is introduced to express an oscillatory contribution from the a-th cell:

$$\Phi_\alpha(t) = \sin(\omega t - \theta_\alpha) + 1 \quad (4)$$

Here, the angular frequency, ω, is identical for all cells where no oscillation occurs at $\omega = 0$ (Figure S7B). The phase difference, θ_a, is defined by the initial configuration (n_x, n_y) of the a-th cell:

$$\theta_\alpha = n_x \Delta\theta + n_y \Delta\theta \quad (5)$$

where, n_x and n_y are row and column indices for the a-th cell in the initial configuration of the cell packing, respectively. θ is a configuration-based phase shift where a synchronous (in-phase) oscillation is reproduced by $\theta = 0$ (Figure S7B).

Supposing that the junctional line between i-th and j-th vertices is shared by the a- and a^*-th cells, the line tension contributed from these two cells at the junction line is expressed as

$$\Lambda_{ij} = p_{ij}\Lambda\left(\Phi_\alpha(t) + \Phi_{\alpha^*}(t) \right), \quad (6)$$

where Λ corresponds to a time-averaged value of the line tension. All model constants are listed in Table 1.

4.6. Image and statistic analysis

Images were quantified by using Fiji (https://fiji.sc/) and Igor Pro. Statistic analyses were performed using Prism6, GraphPad Software, Inc. The statistic test for each analysis is described in the figure legends.

Supplementary Material

Refer to Web version on PubMed Central for supplementary material.

Author Manuscript

Acknowledgements

References

Alt S, Ganguly P, Salbreux G, 2017 Vertex models: from cell mechanics to tissue morphogenesis. Philos. Trans. R. Soc. B Biol. Sci 372, 20150520.

Bertet C, Sulak L, Lecuit T, 2004 Myosin-dependent junction remodelling controls planar cell intercalation and axis elongation. Nature 429, 667–671. [PubMed: 15190355]

Blankenship JT, Backovic ST, Sanny JSP, Weitz O, Zallen JA, 2006 Multicellular rosette formation links planar cell polarity to tissue morphogenesis. Dev. Cell 11, 459–470. [PubMed: 17011486]

Butler MT, Wallingford JB, 2018 Spatial and temporal PCP protein dynamics coordinate cell intercalation during neural tube closure. Elife 7, e36456. [PubMed: 30080139]

Butler MT, Wallingford JB, 2017 Planar cell polarity in development and disease. Nat. Rev. Mol. Cell Biol 18(6), 375–388. [PubMed: 28293032]

Butler MT, Wallingford JB, 2015 Control of vertebrate core planar cell polarity protein localization and dynamics by Prickle 2. Development 142, 3429–39. [PubMed: 26293301]

Chanet S, Miller CJ, Vaishnav ED, Ermentrout B, Davidson LA, Martin AC, 2017 Actomyosin meshwork mechanosensing enables tissue shape to orient cell force. Nat. Commun.

Ciruna B, Jenny A, Lee D, Mlodzik M, Schier AF, 2006 Planar cell polarity signalling couples cell division and morphogenesis during neurulation. Nature 439, 220–224. [PubMed: 16407953]

Farhadifar R, Röper JC, Aigouy B, Eaton S, Jülicher F, 2007 The Influence of Cell Mechanics, Cell-Cell Interactions, and Proliferation on Epithelial Packing. Curr. Biol 17, 2095–2104. [PubMed: 18082406]

Fernandez-Gonzalez R, Zallen JA, 2011 Oscillatory behaviors and hierarchical assembly of contractile structures in intercalating cells. Phys Biol 8, 395–401.

Gardel ML, Schneider IC, Aratyn-Schaus Y, Waterman CM, 2010 Mechanical Integration of Actin and Adhesion Dynamics in Cell Migration. Annu. Rev. Cell Dev. Biol 26, 315–333. [PubMed: 19575647]

Guillot C, Lencuit T, 2013 Mechanics of epithelial tissue homeostasis and morphogenesis. Science 340, 1185–1189. [PubMed: 23744939]

He L, Wang X, Tang HL, Montell DJ, 2010 Tissue elongation requires oscillating contractions of a basal actomyosin network. Nat. Cell Biol 12, 1133–1142. [PubMed: 21102441]

Heisenberg CP, Bellaïche Y, 2013 Forces in tissue morphogenesis and patterning. Cell 153, 948–962. [PubMed: 23706734]

Huang CH, Tang M, Shi C, Iglesias PA, Devreotes PN, 2013 An excitable signal integrator couples to an idling cytoskeletal oscillator to drive cell migration. Nat. Cell Biol 15, 1307–1316. [PubMed: 24142103]

Huebner R, Wallingford JB, 2018 Comning to consencus: A univying model emerges for convergent extension. Dev. Cell 46, 389–396. [PubMed: 30130529]

Inoue Y, Suzuki M, Watanabe T, Yasue N, Tateo I, Adachi T, Ueno N, 2016 Mechanical roles of apical constriction, cell elongation, and cell migration during neural tube formation in Xenopus. Biomech. Model. Mechanobiol 15, 1733–1746. [PubMed: 27193152]

Jenny A, Reynolds-Kenneally J, Das G, Burnett M, Mlodzik M, 2005 Diego and Prickle regulate Frizzled planar cell polarity signalling by competing for Dishevelled binding. Nat. Cell Biol 7, 691–697. [PubMed: 15937478]

Jessen JR, Topczewski J, Bingham S, Sepich DS, Marlow F, Chandrasekhar A, Solnica-Krezel L, 2002 Zebrafish trilobite identifies new roles for Strabismus in gastrulation and neuronal movements. Nat. Cell Biol 4, 610–615. [PubMed: 12105418]

Jiang D, Munro EM, Smith WC, Barbara S, Harbor F, 2005 Ascidian prickle regulates both mediolateral and anterior-posterior cell polarity of notochord cells. Curr. Biol 15, 79–85. [PubMed: 15700379]

Keller R, Davidson L, Edlund A, Elul T, Ezin M, Shook D, Skoglund P, 2000 Mechanisms of convergence and extension by cell intercalation. Philos. Trans. R. Soc. Lond. B. Biol. Sci 355, 897–922. [PubMed: 11128984]

Kim HY, Davidson LA, 2011 Punctuated actin contractions during convergent extension and their permissive regulation by the non-canonical Wnt-signaling pathway. J. Cell Sci 124, 635–646. [PubMed: 21266466]

Maiuri P, Rupprecht JF, Wieser S, Ruprecht V, Bénichou O, Carpi N, Coppey M, De Beco S, Gov N, Heisenberg CP, Lage Crespo C, Lautenschlaeger F, Le Berre M, Lennon-Dumenil AM, Raab M, Thiam HR, Piel M, Sixt M, Voituriez R, 2015 Actin flows mediate a universal coupling between cell speed and cell persistence. Cell 161, 374–386. [PubMed: 25799384]

Mao Y, Baum B, 2015 Tug of war-The influence of opposing physical forces on epithelial cell morphology. Dev. Biol 401, 92–102. [PubMed: 25576028]

Martin AC, Kaschube M, Wieschaus EF, 2009 Pulsed contractions of an actin-myosin network drive apical constriction. Nature 457, 495–499. [PubMed: 19029882]

Nagai T and Honda S, 2001 A dynamic cell model for the formation of epithelial tissues. Philos. Mag. B 81(7), 699–719.

Newman-Smith E, Kourakis MJ, Reeves W, Veeman M, Smith WC, 2015 Reciprocal and dynamic polarization of planar cell polarity core components and myosin. Elife 4, 1–17.

Ninomiya H, Elinson RP, Winklbauer R, 2004 Antero-posterior tissue polarity links mesoderm convergent extension to axial patterning Hiromasa. Nature 430, 364–367. [PubMed: 15254540]

Ossipova O, Kim K, Sokol SY, 2015 Planar polarization of Vangl2 in the vertebrate neural plate is controlled by Wnt and Myosin II signaling. Biol. Open 4, 722–730. [PubMed: 25910938]

Paemka L, Mahajan VB, Ehaideb SN, Skeie JM, Tan MC, Wu S, Cox AJ, Sowers LP, Gecz J, Jolly L, Ferguson PJ, Darbro B, Schneider A, Scheffer IE, Carvill GL, Mefford HC, El-Shanti H, Wood SA, Manak JR, Bassuk AG, 2015 Seizures are regulated by ubiquitin-specific peptidase 9 X-linked (USP9X), a de-ubiquitinase. PLoS Genet 11(3), e1005022. [PubMed: 25763846]

Paré AC, Vichas A, Fincher CT, Mirman Z, Farrell DL, Mainieri A, Zallen JA, 2014 A positional Toll receptor code directs convergent extension in Drosophila. Nature 515, 523–527. [PubMed: 25363762]

Pfister K, Shook DR, Chang C, Keller R, Skoglund P, 2016 Molecular model for force production and transmission during vertebrate gastrulation. Development 715–727. [PubMed: 26884399]

Rauzi M, Lenne PF, Lecuit T, 2010 Planar polarized actomyosin contractile flows control epithelial junction remodelling. Nature 468, 1110–1114. [PubMed: 21068726]

Rauzi M, Verant P, Lecuit T, Lenne PF, 2008 Nature and anisotropy of cortical forces orienting Drosophila tissue morphogenesis. Nat. Cell Biol. 10, 1401–1410. [PubMed: 18978783]

Sawyer JK, Choi W, Jung KC, He L, Harris NJ, Peifer M, 2011 A contractile actomyosin network linked to adherens junctions by Canoe/afadin helps drive convergent extension. Mol. Biol. Cell 22, 2491–2508. [PubMed: 21613546]

Shih J, Keller R, 1992 Cell motility driving mediolateral intercalation in explants of Xenopus laevis. Development 116, 901–914. [PubMed: 1295743]

Shindo A, 2017 Models of convergent extension during morphogenesis. WIREs Dev. Biol e293.

Shindo A, Wallingford JB, 2014 PCP and septins compartmentalize cortical actomyosin to direct collective cell movement. Science. 343, 649–652. [PubMed: 24503851]

Skoglund P, Rolo A, Chen X, Gumbiner BM, Keller R, 2008 Convergence and extension at gastrulation require a myoin IIB dependent cortical actin network. Development 135, 2435–2444. [PubMed: 18550716]

Staple DB, Farhadifar R, Röoer JC, Aigouy B, Eaton S, Jülicher F, 2010 Mechanics and remodelling of cell packings in epithelia. Eur. Phys. J. E 33, 117–127. [PubMed: 21082210]

Sun Z, Amourda C, Shagirov M, Hara Y, Saunders TE, Toyama Y, 2017 Basolateral protrusion and apical contraction cooperatively drive Drosophila germ-band extension. Nat. Cell Biol 19, 375–383. [PubMed: 28346438]

Szabó A, Melchionda M, Nastasi G, Woods ML, Campo S, Perris R, Mayor R, 2016 In vivo confinement promotes collective migration of neural crest cells. J. Cell Biol 213, 543–555. [PubMed: 27241911]

Tada M, Heisenberg CP, 2012 Convergent extension: using collective cell migration and cell intercalation to shape embryos. Development 139, 3897–3904. [PubMed: 23048180]

Tree DRP, Shulman JM, Rousset R, Scott MP, Gubb D, Axelrod JD, 2002 Prickle mediates feedback amplification to generate asymmetric planar cell polarity signaling. Cell 109, 371–381. [PubMed: 12015986]

Walck-Shannon E, Hardin J, 2014 Cell intercalation from top to bottom. Nat. Rev. Mol. Cell Biol 15, 34–48. [PubMed: 24355988]

Wallingford JB, Niswander LA, Shaw GM, Finnell RH, 2013 The continuing challenge of understanding, preventing, and treating neural tube defects. Science. 339, 1222002. [PubMed: 23449594]

Wallingford JB, Rowning BA, Vogeli KM, Rothbächer U, Fraser SE, Harland RM, 2000 Dishevelled controls cell polarity during Xenopus gastrulation. Nature 405, 81–85. [PubMed: 10811222]

Williams M, Yen W, Lu X, Sutherland A, 2014 Distinct apical and basolateral mechanisms drive planar cell polarity-dependent convergent extension of the mouse neural plate. Dev. Cell 29, 34–46. [PubMed: 24703875]

Yin C, Kiskowski M, Pouille PA, Farge E, Solnica-Krezel L, 2008 Cooperation of polarized cell intercalations drives convergence and extension of presomitic mesoderm during zebrafish gastrulation. J. Cell Biol 180, 221–232. [PubMed: 18195109]

Yu JC, Fernandez-Gonzalez R, 2017 Quantitative modelling of epithelial morphogenesis: integrating cell mechanics and molecular dynamics. Semin. Cell Dev. Biol 67, 153–160. [PubMed: 27481581]

Zallen JA, Wieschaus E, 2004 Patterned gene expression directs bipolar planar polarity in Drosophila. Dev. Cell 6, 343–355. [PubMed: 15030758]

Highlights:

- Anteroposterior neighboring cells display asynchronous actomyosin oscillations during convergent extension in the *Xenopus* mesoderm.

- Mathematical modeling shows the asynchronous oscillation with an optimal frequency is important for convergent extension.

- PCP protein Prickle 2 displays both spatial and temporal patterns of localization to the contracting cell-cell junctions.

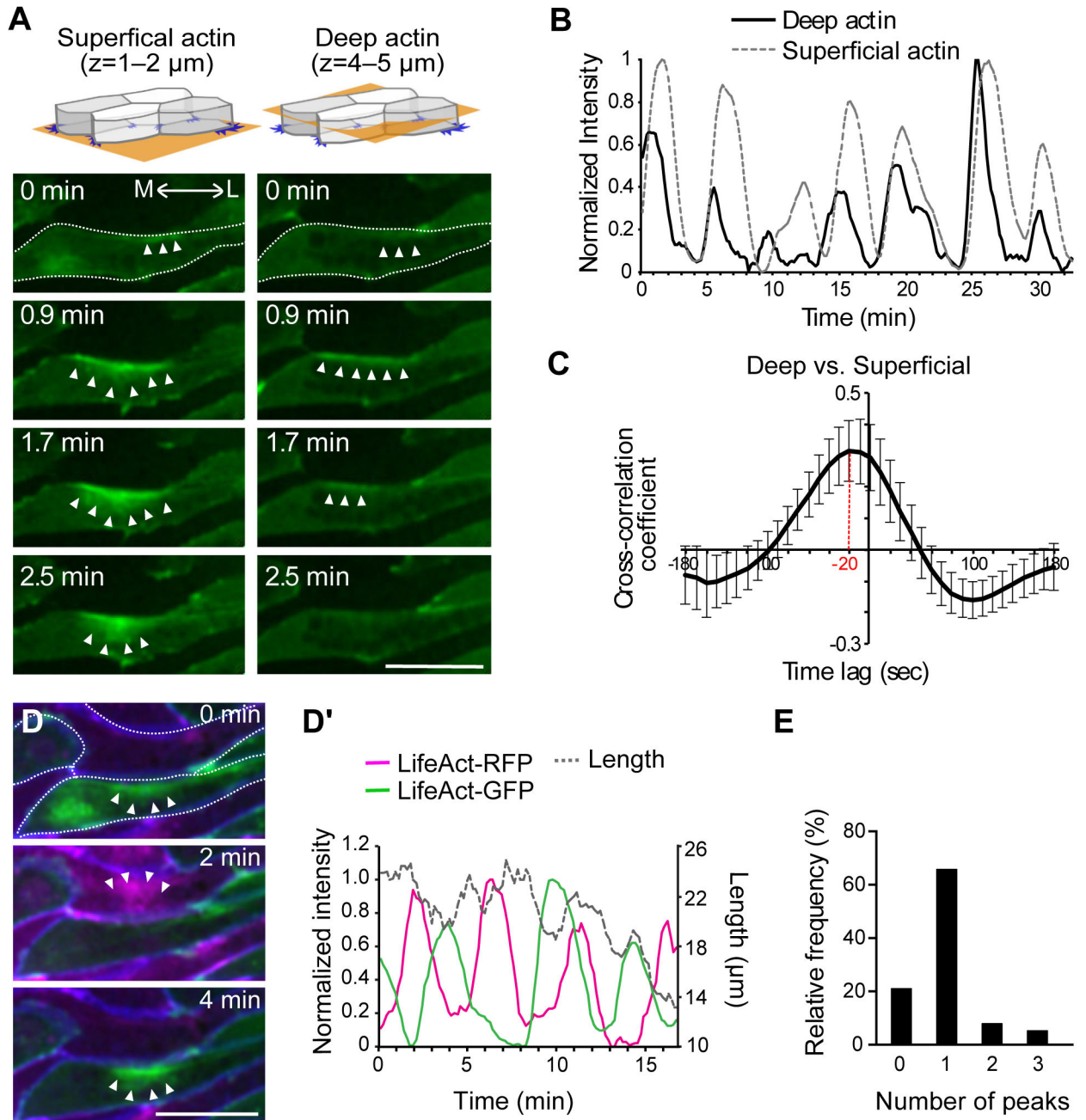- Prickle 2 is required for controlling the frequency of actomyosin oscillations.

A

Superfical actin
(z=1–2 µm)

Deep actin
(z=4–5 µm)

B

C

Deep vs. Superficial

D

D'

E

Figure 1. Actomyosin oscillations during convergent extension of the *Xenopus* dorsal mesoderm.
(**A**) Mosaic expression of LifeAct-GFP (F-actin marker) allows imaging of labeled cells apposed to unlabeled cells for unambiguous assessment of actin dynamics in the superficial (left) and deep (right) actin populations. Stills from time-lapse movies show the progression of actomyosin flow across time and space (arrowheads). M: medial, L: lateral. Dotted line outlines the cell. (**B**) Peaks of normalized actin intensity allow quantification of actomyosin dynamics in the deep and superficial populations along contracting v-junctions from a single cell. (**C**) Actomyosin oscillations in deep and superficial populations are synchronous, showing a significant cross-correlation. (**D, D'**) Two-color labeling of F-actin in same cells

in panel A with membrane-BFP reveals that oscillations along shared v-junctions (See Figure S1A) in apposed cells are out of phase; quantification of normalized intensity together with junction length over time is displayed at right. The cells are outlined with a dotted line. **(E)** The number of LifeAct's peaks observed in a given cell between any two peaks occurring in an adjacent cell shows pulses in neighboring cell display a roughly one-to-one ration (See Figure S6). Scale bar = 20 μm
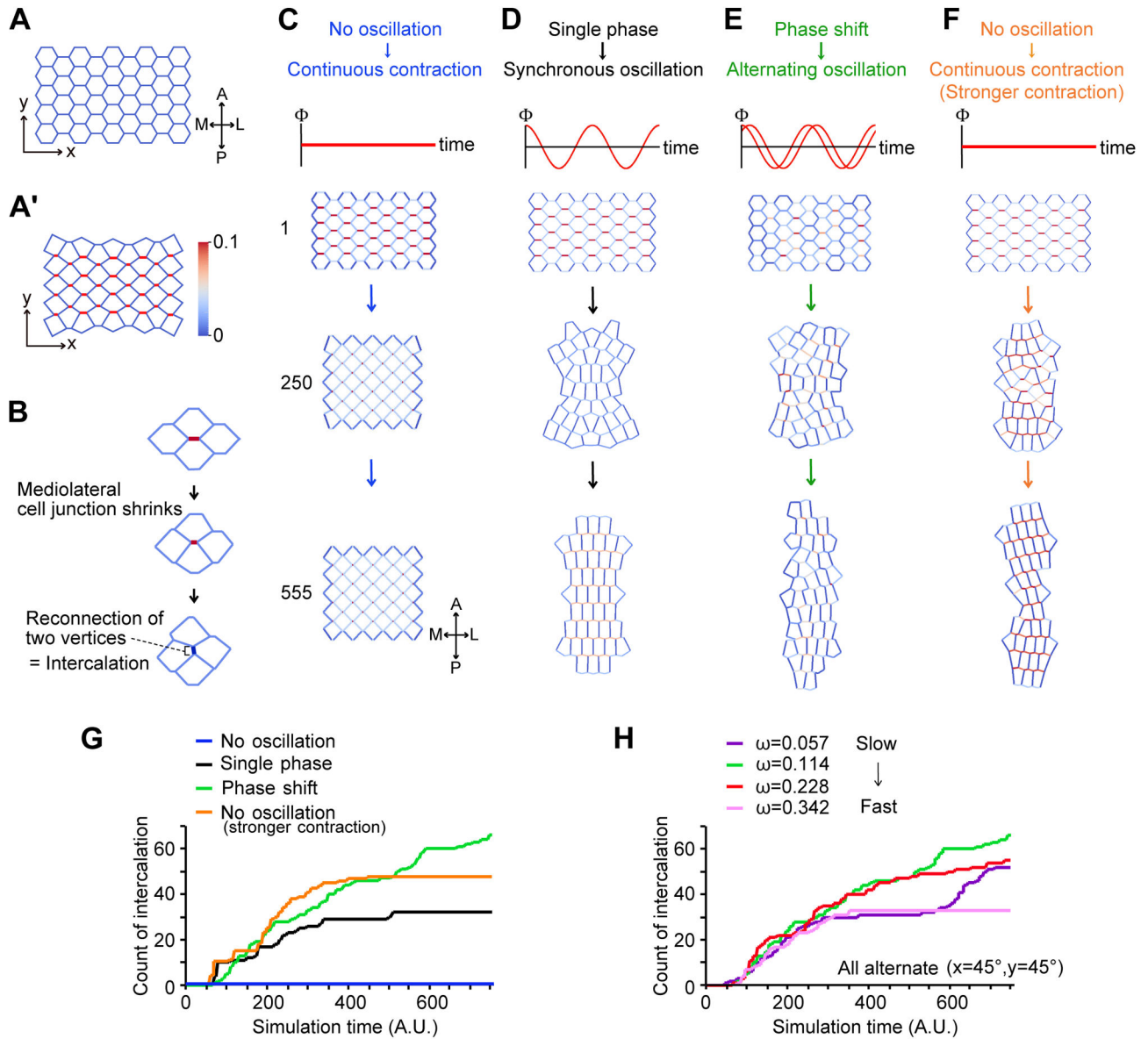
Figure 2. A 2D vertex model reveals that the alternate, carefully timed contractions are a general feature of cell intercalation.
(A) Initial cell arrangement used in the simulations. Vertical axis (x) indicates antero (A) - posterior (P), and horizontal axis (y) indicates medio (M) – lateral (L). **(A')** Example of junction contractions. The cell-cell junctions aligned along the mediolateral axis (x-axis) can contract in the model. The edge color indicates the magnitude of the line tension of the cell and cell junction (red=maximum strength, blue=minimum strength). **(B)** Example of the junction remodeling in the simulations. After the cell-cell junction shows emergence of a new junction, and is counted as one intercalation, as shown in Figures 2G and 2H. **(C)** Simulation of CE with coincident, continuous contraction without oscillation generates no intercalation. Top panel shows cells at 1 simulation time t = 1 (A.U); middle panels at t = 250 and lower panels at t = 555. **(D)** Synchronous oscillating contractions (In-phase oscillation) generate modest intercalation. **(E)** Alternate oscillating contractions generate

robust intercalation. **(F)** Continuous contraction without oscillating at 1.5 times the line tension generates modest intercalation. (G) Graph of intercalation quantified by the number of newly formed cell-cell junctions after complete v-junction shortening as shown in Figure 1B, representing the efficiency of cell intercalation. Blue: continuous contraction ($\Lambda = 0.10$); Black: Synchronous oscillation ($\Lambda = 0.10$); Green: alternating oscillation ($\Lambda = 0.10$); Orange: continuous contraction ($\Lambda = 0.15$). Frequency of oscillation is defined by angular frequency $\boldsymbol{\omega}$ [radian/simulation time unit] ($\boldsymbol{\omega} = 2\pi/T$, See experimental procedures). For both synchronous and alternating oscillations, $2\pi/T$ is fixed to 0.114. The phase shift to generate alternating oscillation is defined by $\theta_x=0.7854$, $\theta_y=0.7854$ (see experimental procedure). **(H)** Effect of oscillating frequency on intercalation efficiency for alternating oscillation. Purple: $\boldsymbol{\omega} = 0.057$ (slowest), Green: $\boldsymbol{\omega} = 0.114$, Red: $\boldsymbol{\omega} = 0.228$, Pink: $\boldsymbol{\omega} = 0.342$ (Fastest). The phase shift is fixed to $\theta = 2.5\pi \times 10^{-1}$ for the three groups.
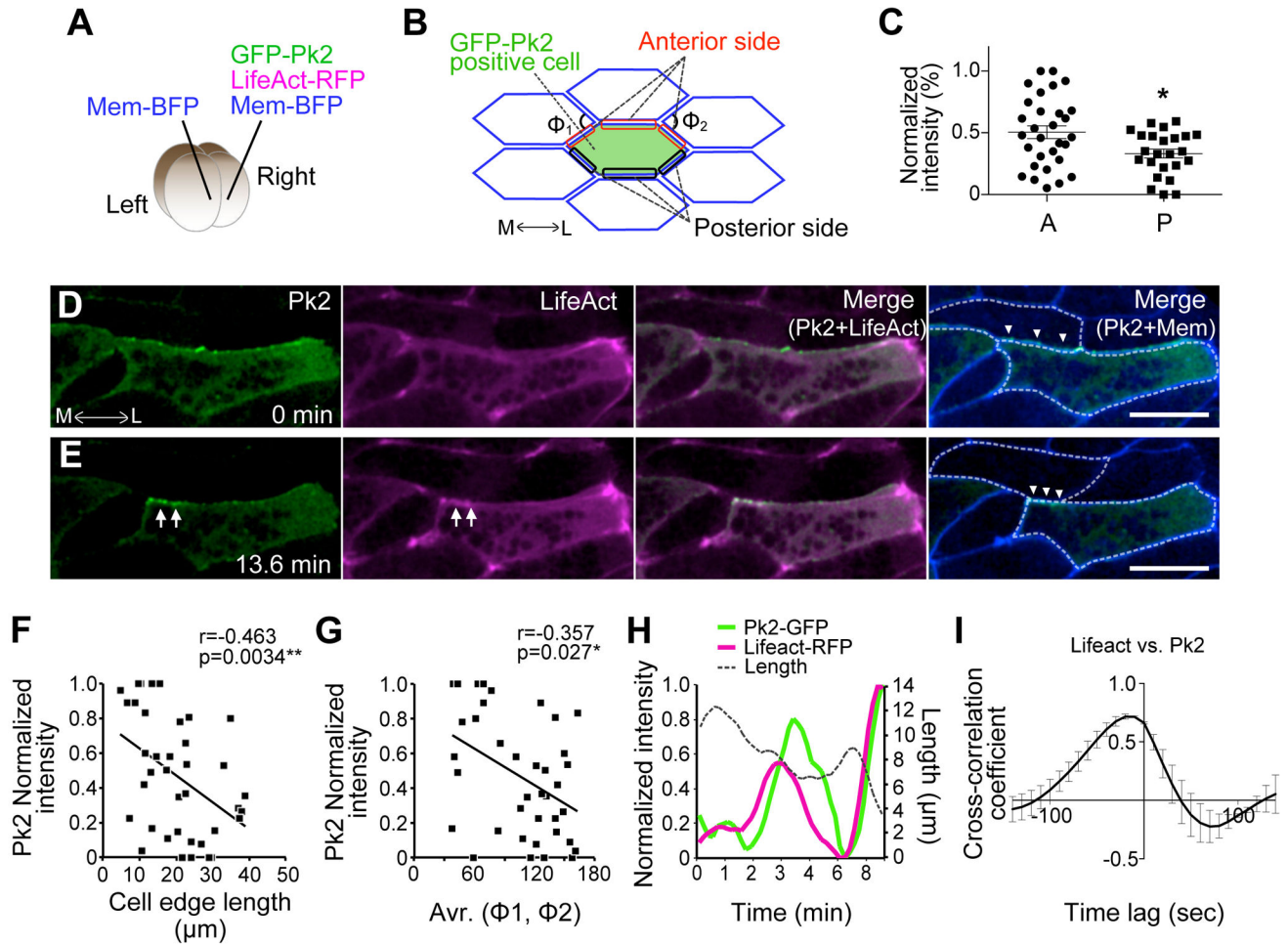
Figure 3. Prickle2 displays temporal and spatial patterns of localization during cell intercalation.
(**A**) Method for mosaic expression of GFP-Pk2, LifeAct-RFP, and membrane (Mem) -BFP in a *Xenopus* embryo at 4 cell stage. (**B**) Scheme showing the cell and cell-cell junctions measured for analysis in C, F, G, and H. The angle of apices of neighboring cells attached to a shrinking junction is indicated as Φ. (**C**) Mean intensity of GFP-Pk2 on anterior and posterior cell cortices. [* p = 0.0282, Student's *t*-test; anterior (A): n = 30, posterior (P): n = 25] (**D, E**) Still images from time-lapse movie of GFP-Pk2 during junction shrinkage. Images of E are 13.6 minutes after the images in D. Arrowheads indicate contracting v-junction; arrows indicate the accumulation of GFP-Pk2 at the anterior face of the contracting v-junction. (**F**) Correlation between GFP-Pk2 intensity and the length of cell-cell junctions. GFP-Pk2 intensity is converted to percentages in each image. (38 junctions from 2 embryos). (**G**) Correlation between GFP-Pk2 intensity and the angle Φ. Same numbers as (F). (**H**) Quantification of normalized intensity of LifeAct (magenta) and Pk2-GFP (green) together with junction length over time from single contracting cell junction. (I) Synchronous accumulation of F-actin and Pk2 is shown by cross correlation. Scale bar = 20 μm.
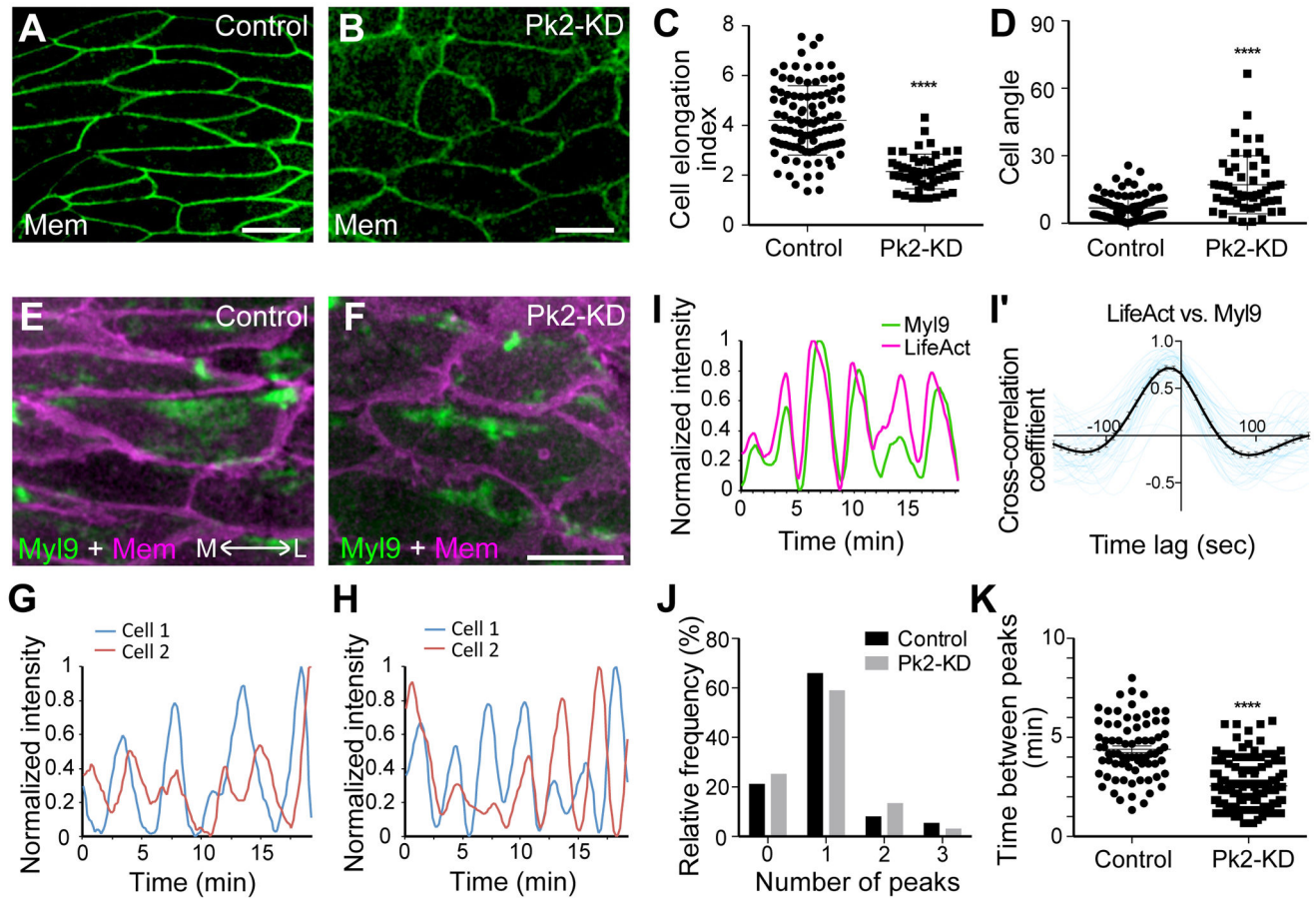
Figure 4. Prickle 2 controls the frequency of actomyosin pulses.
(**A, B**) Cells expressing membrane (Mem) -GFP in the *Xenopus* dorsal mesoderm display an
elongate and aligned morphology in control (A). Pk2-KD disrupts elongation and orientation
of cells (B). (**C, D**) Quantification of cell shapes and orientations by measuring length-width
ratio (ellipticity) of each cell and cell angle from mediorateral axis, respectively. (Cell
elongation index: **** p < 0.0001, Student *t*-test, control: n = 100 from three embryos, Pk2-
KD: n = 51 from three embryos; Orientation: **** p < 0.0001, Mann Whitney U-test,
control: n = 97 from three embryos, Pk2-KD: n = 51 from three embryos). (**E, F**) Still
images from time-lapse movies of Myl9-GFP and Mem-RFP in control (E) or Pk2-KD (F).
(**G, H**) Representative oscillations of Myl9 intensity in two apposed cells (cell1 and cell2,
see Figure S4B) in a control (G) or Pk2-KD (H). (**I**) Normalized intensities of Myl9-GFP
and LifeAct-RFP, measured along mediolaterally aligned cell junctions in Pk2-KD embryos.
(**I'**) Cross-correlation of normalized intensities of Myl9 and LifeAct along medioraterally
aligned cell junctions in Pk2-KD embryos revealed their synchronized oscillations (black
line with SE). Each blue line is from each cell junction. (**J**) Peaks in apposed cells generally
display a one-to-one ration, suggesting a roughly asynchronous and alternate relationship
between cell neighbors. To compare, the result from control embryos in Figure 1E is added.
See also Figure S6. (**K**) Time between peaks is significantly reduced after Pk2-KD. **** p <

0.0001, Mann Whitney U-test, control: n = 76 from three embryos, Pk2-KD: n = 138 from three embryos. Scale bar = 20 μm.

Table 1.

Model parameters

Symbol	Value	Descriptions
K_a	1.0	Area elasticity of Eq. (2)
Γ_α	−6.0	Peripheral contractility of Eq. (2)
Λ	{0.10, 0.15}	Mean value of line tension of Eq. (6)
$A_\alpha^{(0)}$	2.6	Cell area at stress free state of Eq. (2)
ω	{0, 0.57, 1.14, 2.28, 3.42} $\times 10^{-1}$	Angular frequency of Eq. (4)
θ	{0.0, $2.5\pi \times 10^{-1}$}	Configuration-based phase shift of Eq. (5)
η	1.0	Friction coefficient of Eq. (1)
t	1.0×10^{-1}	Time step size for numerical integration of Eq. (1)